

Fine-scale oscillations in the wavelength- and intensity-dependence of high-harmonic generation: connection with channel closings

K. L. Ishikawa,^{1,2,*} K. Schiessl,³ E. Persson,³ and J. Burgdörfer³

¹*Integrated Simulation of Living Matter Group, RIKEN Computational Science Research Program, 2-1 Hirosawa, Wako, Saitama 351-0198, Japan*

²*PRESTO (Precursory Research for Embryonic Science and Technology), Japan Science and Technology Agency, Honcho 4-1-8, Kawaguchi-shi, Saitama 332-0012, Japan*

³*Institute for Theoretical Physics, Vienna University of Technology, Wiedner Hauptstraße 8-10, A-1040 Vienna, Austria, EU*

(Dated: February 3, 2022)

We investigate the connection of recently identified fine-scale oscillations in the dependence of the yield of the high-harmonic generation (HHG) on wavelength λ of a few-cycle laser pulse [K. Schiessl, K.L. Ishikawa, E. Persson, and J. Burgdörfer, Phys. Rev. Lett. **99**, 253903 (2007)] to the well-known channel closing (CC) effect. Using the Lewenstein model of HHG, we identify the origin of the oscillations as quantum interference of many rescattering trajectories. By studying the simultaneous variations with intensity and wavelength, different models for the interference of channel closing peaks can be tested. Contrary to theoretical predictions for short-range potentials, the peaks are not located neither at nor just below the CC condition, but a significant shift is observed. The long Coulomb tail of the atomic potential is identified as the origin of the shift.

PACS numbers: 32.80.Rm, 42.65.Ky, 32.80.Fb

I. INTRODUCTION

High harmonic generation (HHG) represents a versatile and highly successful avenue towards an ultrashort coherent light source covering a wavelength range from the vacuum ultraviolet to the soft X-ray region [1]. This development has opened new research areas such as attosecond science [2, 3] and nonlinear optics in the XUV region [4, 5]. The fundamental wavelength λ used in most HHG experiments to date is in the near-visible range (~ 800 nm). The cutoff law for the harmonic spectrum $E_c = I_p + 3.17U_p$, where I_p denotes the binding energy of the target atom and $U_p = F_0^2/4\omega^2 = F_0^2\lambda^2/16\pi^2$ the ponderomotive energy (F_0 : laser electric field strength), suggests that a longer fundamental wavelength would be advantageous to extend the cutoff to higher photon energies, since U_p increases quadratically with λ . This has stimulated an increasing interest in the development of high-power mid-infrared (~ 2 μ m) laser systems, e.g., based on optical parametric chirped pulse amplification. The first generation of water-window harmonics with clear plateau and cut-off structures has recently been reported [9]. Along those lines the dependence of the HHG yield on λ has become an issue of major interest [6, 7, 8, 10, 14]. It had long been believed that the spreading of the returning wavepacket would result in a λ^{-3} dependence of the HHG efficiency [11] as long as ground state depletion can be neglected [12]; experimental findings [13] provided partial support. Recently, however, Tate *et al.* [14] have reported a different wavelength-scaling of HHG between 800 nm and 2 μ m calculated

with the time-dependent Schrödinger equation (TDSE) for Ar and a strong-field approximation (SFA) for He. They found the yield to be described by a power-law $\propto \lambda^{-x}$ with $5 \leq x \leq 6$. Investigating the λ dependence on the level of single-atom response for H and Ar by numerically solving the time-dependent Schrödinger equation we could confirm the overall scaling with an inverse power law exceeding five [6], the harmonic yield was found not to depend smoothly on the fundamental wavelength, but to exhibit surprisingly rapid oscillations with a period of 6–20 nm depending on the wavelength region. A semiclassical analysis based on the SFA has revealed that the rapid oscillations are due to the interference of five to ten different rescattering trajectories [6]. Moreover, we found the oscillations to be stable with respect to variations of the pulse envelope as long as the effective pulse length and thus the number of relevant trajectories remains equal, while the amplitude of the oscillations decreases with decreasing pulse length [8]. These observations underscored the view that the oscillations are due to the interference of quantum paths.

Oscillations of the HHG yield have previously been reported in terms of the dependence on the intensity of the driving laser $I_0 \propto F_0^2$, both experimentally [15, 16] and theoretically [17, 18]. Borca *et al.* [17] and Milošević and Becker [18] have shown that HHG is enhanced at channel closings (CC), i.e., when

$$R = \frac{I_p + U_p}{\hbar\omega}, \quad (1)$$

is an integer. Channel closing in this context refers to the threshold for multiphoton ionization in a laser field. Most of these theoretical studies employed zero-range potentials or the SFA which both neglect the influence of the long-range potential on the ionized electron.

*Electronic address: ishiken@riken.jp

Frolov *et al.* [7] have recently analyzed the wavelength-dependence of HHG in terms of channel closings (or threshold phenomena). They have calculated the harmonic yield using the time-dependent effective range theory, and shown that the peaks of the yield oscillation around $\lambda = 1 \mu\text{m}$ coincide with integer values of R if an effective ionization potential \tilde{I}_p (e.g., 10.5 eV for H) is used in place of I_p in Eq. (1). This method is, however, strictly applicable only for short-range potentials and also neglects the excited atomic states. On the other hand, we have recently found [8] channel closing peaks in the TDSE-calculated HHG yields around $1 \mu\text{m}$ and $2 \mu\text{m}$ wavelengths which are characterized by a spacing of $\delta R = 1$, as expected from the CC picture, when the true ionization potential I_p is used.

In the present paper, we study the connection between the oscillation in the wavelength-dependence of the HHG yield and the channel-closing in more detail. We study the harmonic spectrum in the two-dimensional parameter space of intensity I_0 and driver wavelength λ_c . We compare the results of the full 3D TDSE solution with the strong-field approximation and a truncated Coulomb-potential model in order to delineate underlying mechanisms. We find that the correspondence of the modulation period to $\delta R = 1$ holds for a wide wavelength range between 800 nm and $2 \mu\text{m}$, and that the peak positions in terms of R are almost independent of laser intensity. The systematic displacement of the peak positions relative to integer values is found to be consistent with the effect of the long-range Coulomb tail on the returning electron.

The present paper is organized as follows. Section II summarizes the two complementary integration schemes employed for a full numerical solution of the TDSE. In Sec. III we discuss the overall wavelength dependence at a fixed value of fundamental intensity all the way from $\lambda = 800 \text{ nm}$ to $2 \mu\text{m}$. We also analyze small-scale oscillations in terms of quantum-path interference based on the saddle-point analysis (SPA) [11, 18]. In Sec. IV we investigate the variation of the λ -dependence of HHG with intensity and pulse shape. In Sec. V we discuss the period of the oscillations in terms of the channel-closing number R and investigate its robustness against the variation of the wavelength region, the driver intensity, and pulse shape. In Sec. VI we discuss the origin of the peak shift from integer R values and clarify how the Coulomb tail of the atomic potential affects the peak position. Conclusions are given in Sec. VII. Atomic units are used throughout the paper unless otherwise stated.

II. NUMERICAL METHODS

We solve the atomic time-dependent Schrödinger equation (TDSE) in the length gauge for a linearly polarized laser field with the central wavelength $\lambda_c = 2\pi c/\omega$,

$$i\frac{\partial}{\partial t}\psi(\mathbf{r}, t) = \left[-\frac{1}{2}\nabla^2 + V_{\text{eff}}(r) + zF(t)\right]\psi(\mathbf{r}, t), \quad (2)$$

where $F(t) = F_0 f(t) \sin(\omega t)$ denotes the laser electric field, $f(t)$ is the envelope function and $V_{\text{eff}}(r)$ the atomic potential. For hydrogen (H), $V_{\text{eff}}(r)$ is the bare Coulomb potential while for argon (Ar) we employ a model potential [19] within the single-active electron approximation which reproduces the binding energy to an accuracy of typically $\approx 10^{-3}$. We employ two complementary methods to solve Eq. (2) in order to establish reliable and consistent results.

In the first method, Eq. (2) is numerically integrated using the alternating direction implicit (Peaceman-Rachford) method [20] with a uniform grid spacing Δr being dependent on the numerical problem in the range of $10^{-2} \leq \Delta r \leq 6.25 \times 10^{-2} \text{ a.u.}$ In general, a finer grid spacing is needed for a longer wavelength, and also for Ar than for H. In order to reduce the difference between the discretized and analytical wave function, we scale the Coulomb potential by a few percent at the first grid point [21]. The time step Δt is typically $1/16000$ of an optical cycle for 800 nm wavelength, i.e., $6.895 \times 10^{-3} \text{ a.u.}$ This algorithm is accurate to the order of $\mathcal{O}(\Delta t^3)$. In the second method, the TDSE is integrated on a finite grid by means of the pseudo-spectral method [22] which is also accurate to the order of $\mathcal{O}(\Delta t^3)$. It allows for larger time steps of the order of 0.1 atomic units. The r coordinate is discretized within the interval $[0, r_{\text{max}}]$ with a non-uniform mesh point distribution. The innermost grid point is typically as small as $2.5 \times 10^{-4} \text{ a.u.}$, enabling an accurate description near the nucleus. A smooth cut-off function is multiplied at each time-step to avoid spurious reflections at the border r_{max} , while another cut-off function prevents reflections at the largest resolved energy E_{max} . For Ar the occupied states supported by the model potential are dynamically blocked during the time evolution by assigning a phase corresponding to an unphysically large and positive energy eigenvalue [23]. We calculate the dipole acceleration $\ddot{d}(t) = -\partial_t^2 \langle z(t) \rangle$, employing the Ehrenfest theorem through the relation $\ddot{d}(t) = \langle \psi(\mathbf{r}, t) | \cos \theta / r^2 - F(t) | \psi(\mathbf{r}, t) \rangle$ [22], where the second term can be dropped as it does not contribute to the HHG spectrum.

For the wavelength-dependence of the harmonic yield, in particular the global scaling, it is important to specify the definition of the integral yield. One can focus on a given number of harmonic orders, on a fixed energy interval, or the entire spectrum. Following Refs. [6, 7, 8, 14], we consider in this work the HHG yield defined as energy radiated from the target atom (single-atom response) per unit time [25] integrated for a fixed photon energy range, specifically from 20 to 50 eV:

$$\Delta Y = \frac{1}{3c^3 T} \int_{20 \text{ eV}}^{50 \text{ eV}} |a(\omega)|^2 d\omega, \quad (3)$$

where T denotes the pulse duration. Note that the energy window ΔE of the output radiation (here 20 to 50 eV) is kept constant when analyzing ΔY as a function of λ . Clearly, both the number and order of the harmonic

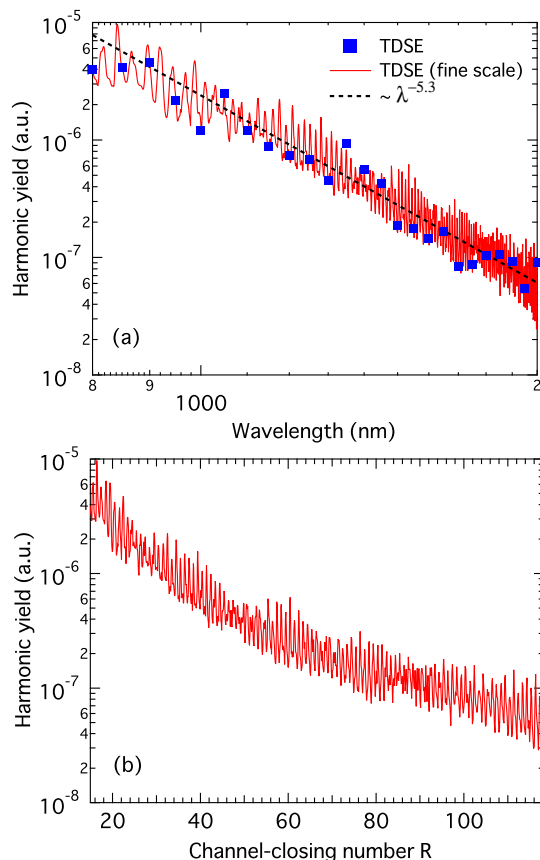


FIG. 1: (Color online) Wavelength dependence of the integrated harmonic yield ΔY between 20 and 50 eV as a function of (a) wavelength λ and (b) channel-closing number R . ■ : TDSE results obtained by the pseudo-spectral method. In addition, results on a fine scale (solid line) are presented. Dashed line: fit $\Delta Y \propto \lambda^{-5.3}$.

peaks lying in the fixed energy interval change as λ_c is varied.

III. WAVELENGTH DEPENDENCE

We adopt the laser parameters of Ref. [14], with a fixed peak intensity of 1.6×10^{14} W/cm², a variation of λ between 800 nm and 2 μ m, and an envelope function $f(t)$ corresponding to an 8-cycle flat-top sine pulse with a half-cycle turn-on and turn-off.

Figure 1 displays the HHG yield for atomic hydrogen calculated on a fine mesh in λ with a spacing of 1 nm. Superimposed on a global power-law dependence $\Delta Y \propto \lambda^{-x}$ ($x \approx 5$) [6, 7, 8, 14], we find remarkably strong and rapid fluctuations through the entire λ range. The origin of this oscillation can be identified as the quantum interference of up to ten rescattering trajectories, based on the SFA analysis [6, 8].

The effect of the interference of multiple quantum paths was previously studied in the context of the *inten-*

sity dependence of HHG and above-threshold ionization (ATI) [16, 17, 18]. Using the quasistationary quasienergy state theory for a zero-range potential and the strong-field approximation, Borca *et al.* [17], and Milošević and Becker [18] have shown that HHG exhibits resonance-like enhancement when N -photon ionization channel is closed with increasing intensity, i.e. the parameter R (Eq. (1)) becomes an integer. Zaïr *et al.* [16] have very recently reported experimental observation of the oscillation in the intensity dependence of the HHG yield as evidence of the interference between the short and long paths. The analysis in Ref. [18] may be applied to the wavelength-dependence as well, suggesting to look at our results in terms of R . Data of Fig. 1(a) are replotted in terms of R in Fig. 1(b), which permits a detailed analysis of the channel closing behavior (see below).

In Figs. 2 and 3 we reexamine the role of quantum paths in the oscillations of the wavelength-dependence of the harmonic yield as a function of R on a finer R scale. We compare full TDSE solutions with approximations based on the strong field approximation (SFA) [11, 29]. We first apply the Gaussian model [11], in which the ground-state wave function has the form

$$\psi(\mathbf{r}) = \left(\frac{\alpha}{\pi}\right)^{3/4} e^{-\alpha r^2/2}, \quad (4)$$

where α is chosen to reproduce I_p . An appealing point of the Gaussian model is that the dipole transition matrix element also takes a Gaussian form [11],

$$\mathbf{d}(\mathbf{p}) = i \left(\frac{1}{\pi\alpha}\right)^{3/4} \frac{\mathbf{p}}{\alpha} e^{-\mathbf{p}^2/2\alpha}, \quad (5)$$

and that one can evaluate the integral with respect to momentum in the formula for the dipole moment (Eq. (8) of Ref. [11]) analytically, without explicitly invoking the notion of quantum paths. Unphysically rapid decrease for $\mathbf{p}^2/2\alpha \gg 1$ limits the application of Eq. (5) to harmonic orders with momenta of the returning electron not substantially exceeding $\mathbf{p}^2/2\alpha \approx 1$. We have confirmed that the resulting harmonic spectra have an adequate plateau and cut-off structure for the value of α (1 and 2 a.u.) used in the present study. The obtained wavelength dependence of the HHG yield, expressed in terms of R (Fig. 2 (b)), exhibits oscillations similar to that in the TDSE result (Fig. 2 (a)), although peaks are found - contrary to TDSE results - near integer values of R . In addition we employ complex solutions of the saddle-point approximation (SPA) [18], while we have previously obtained similar results by employing classical trajectories [6, 8]. Up to 16 possible trajectories for each individual photon energy are considered. When including up to ten and twelve returning paths for the case of H and Ar, respectively, the SPA can reproduce the modulation depth and frequency of the λ oscillations of the TDSE and the Gaussian model reasonably well, thus strongly supporting the quantum path interference as the origin of the fluctuations. The SPA result for Ar with twelve

trajectories (Fig. 3 (b)) reproduces even the small peaks between the main peaks.

We emphasize the remarkable variation on a fine λ scale. One might suspect that the oscillation as in Figs. 1–3 would be specific to monochromatic driver pulses and smeared out for the case of ultrashort broadband pulses. The pulse shape used in this study is, however, not monochromatic but its spectral width $\Delta\lambda$ is $\sim 10\%$ of λ_c . The rapid variations of the harmonic yield occur on a scale $\delta\lambda$ much smaller than this width. This finding, at a first glance surprising, is a direct consequence of the quantum path interference. It follows from the existence and the fixed spacing in between discrete points in time - controlled by λ_c - at which electronic trajectories are launched. As long as the few-cycle pulse permits the generation of a set of a few quantum paths in subsequent half-cycles, the overall temporal characteristics of the driver pulse is of minor importance. We have also checked that the fluctuations in the harmonic yield are not an artefact of our particular choice of $f(t)$. They can be observed also for “smoother” pulse shape such as \sin^2 and Gaussian pulses as well as shorter pulses, provided that the pulse can support multiple returning trajectories (Fig. 4). The temporal profile of the pulse influences the detailed shape of the interference pattern, in particular the amplitude of the oscillations decreases with decreasing pulse length due to the reduction of the effective number of returning electron trajectories.

IV. INTENSITY DEPENDENCE

Previous work [16, 17, 18] studied the intensity dependence of the HHG yield at a fixed value of fundamental wavelength λ_c . On the other hand, we have so far focussed on the wavelength dependence at a fixed value of intensity ($1.6 \times 10^{14} \text{ W/cm}^2$). We extend now this analysis to the two-dimensional parameter plane (λ_c, I_0) in order to explore the underlying mechanisms in more detail. An example for hydrogen (Fig. 5) for a narrow interval of wavelength ($1 \mu\text{m} \leq \lambda_c \leq 1.1 \mu\text{m}$) and intensity ($1.3 \times 10^{14} \text{ W/cm}^2 \leq I_0 \leq 1.6 \times 10^{14} \text{ W/cm}^2$) displays regularly shaped ridges each of which can be mapped onto a fixed channel closing number R . This regularity is also reflected in the cuts through this two-dimensional data for different fixed intensities for both hydrogen (Fig. 6 (a)) and argon (Fig. 6 (b)).

Not only the peak positions but also detailed structures of the dependence on λ_c are quite robust against the variation of I_0 , when expressed in terms of R . For later reference we stress that these remarkable observations hold true only when the channel-closing (CC) number R is determined with the *true ionization potential* (Eq. (1)); the use of any other value of effective ionization potential would shift each peak and consequently each curve in Fig. 6 by a different amount. This can also be understood from the fact that lines of constant values of $(U_p + \tilde{I}_p)/\hbar\omega$ (with e.g. $\tilde{I}_p = 10.5 \text{ eV}$) in Fig. 5 (b)

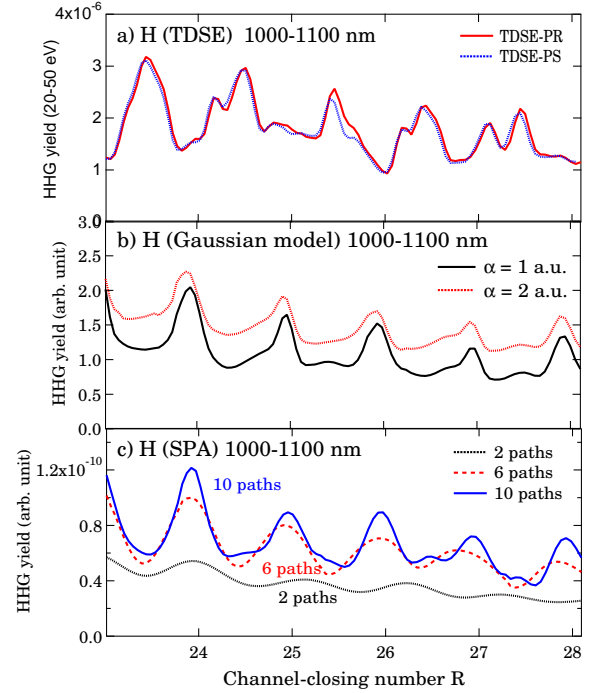


FIG. 2: (Color online) Variations of the integrated harmonic yield (20 to 50 eV) in a narrow range of $\lambda = 1000 - 1100 \text{ nm}$, as a function of R , for H. a) comparison between the TDSE solutions with the Peaceman-Rachford (PR) and the pseudo-spectral (PS) methods. b) the results of the Gaussian model with $\alpha = 1 \text{ a.u.}$ (solid) and 2 a.u. (dotted). c) build-up of the interference pattern with increasing number of quantum trajectories within the SPA. In b) and c) the vertical axis is in arbitrary units.

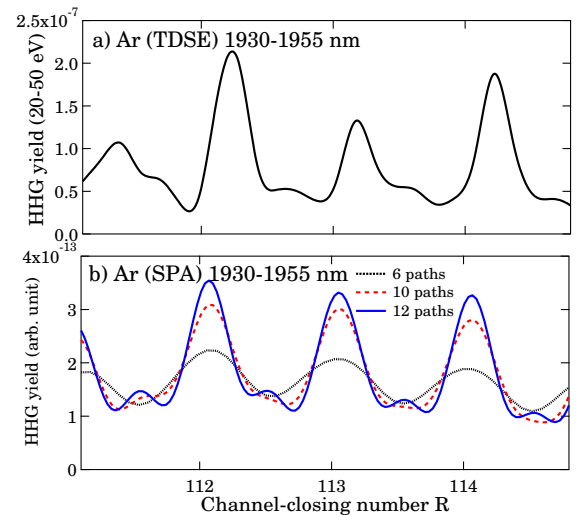


FIG. 3: (Color online) Variations of the integrated harmonic yield (20 to 50 eV) in a narrow range of $\lambda = 1930 - 1955 \text{ nm}$, as a function of R , for Ar. a) the TDSE solution, b) build-up of the interference pattern with increasing number of quantum trajectories within the SPA.

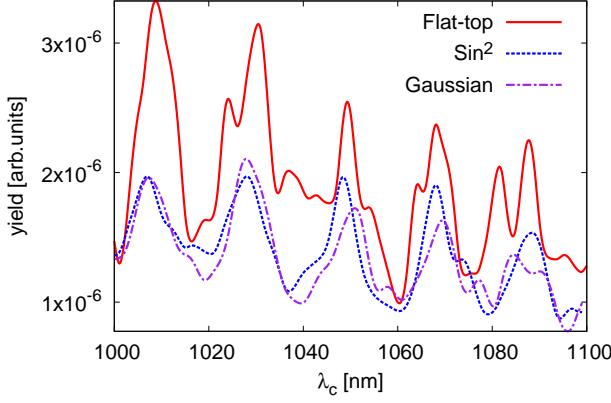


FIG. 4: (Color online) Fluctuations of the harmonic yield ΔY as a function of the fundamental wavelength λ for hydrogen. Solid: 8-cycle flat-top with a 1/2 (1/2) cycle ramp on (off), dotted: 14-cycle \sin^2 pulse with a FWHM of $\tau_p = 7$ cycles, dash-dotted: 16-cycle Gaussian with a FWHM of $\tau_p = 7$ cycles. Other pulse parameters are the same as in Fig. 1.

deviate from the ridges which manifest as peaks along lines of constant I_0 (Fig. 6 (a)). Results for argon (Fig. 6 (b)) show a similar behavior, indicating the applicability of the parameter R independent of the atomic species.

V. MODULATION PERIOD

The modulation period $\delta\lambda$ of the harmonic yield is a function of the central wavelength λ_c itself. With increasing λ_c , $\delta\lambda$ decreases from about 30 nm near 800 nm wavelength to ≈ 6 nm near a wavelength of $2 \mu\text{m}$ (Fig. 7). However, expressed in terms of the channel closing number R , the separation of the principal peaks is given by $\delta R = 1$ both for the TDSE and the SPA results (see Figs. 2 and 3). Interference peaks appear with this spacing regardless of intensity (Fig. 6). The peaks in the TDSE results are, however, *not* located at integer values of R , as opposed to the SPA results as well as previous theoretical work [17, 18]. This problem was previously encountered in the intensity-dependence of HHG and ATI [31]. In order to recover integer values the use of an effective ionization potential \tilde{I}_p in place of I_p in Eq. (1) was proposed based on arguments that either the enhancement was due to multiphoton resonances with ponderomotively upshifted Rydberg states [32] (\tilde{I}_p corresponds to the excitation energy of the resonant state) or that high-lying atomic states are strongly distorted by an intense laser field to form a quasicontinuum, effectively lowering the ionization potential [7]. As long as one considers only the intensity-dependence at a fixed wavelength, the difference $\Delta\tilde{I}_p = \tilde{I}_p - I_p$ causes a constant shift of R by $\Delta\tilde{I}_p/\omega$. Consequently, integer values of R could be restored along this axis for a suitable choice of \tilde{I}_p . However, considering now the wavelength-dependence at a

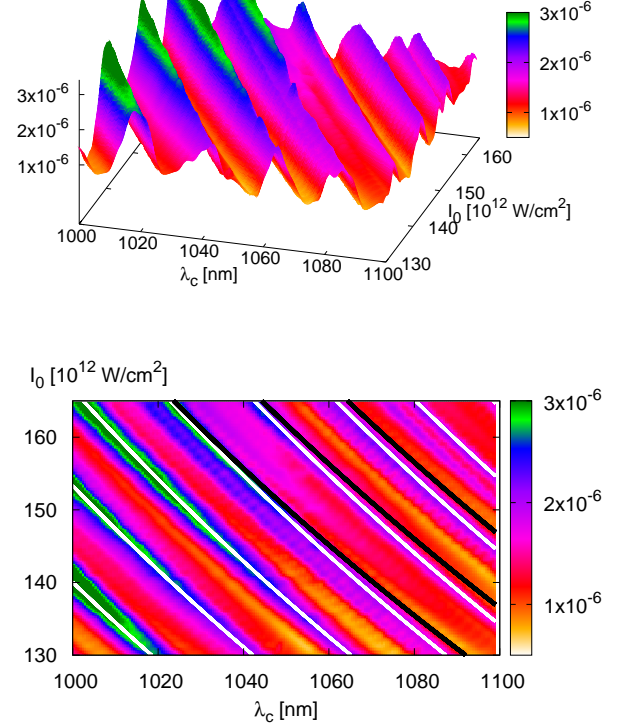


FIG. 5: (Color online) TDSE-calculated integrated harmonic yield between 20 and 50 eV for H (8-cycle flat-top pulse) in the (λ_c, I_0) plane. In the contour plot (lower panel), white lines show values of constant $(U_p + I_p)/\hbar\omega$, shifted from integer values by +0.52, while black lines (only three are shown for clarity) represent values of constant $(U_p + \tilde{I}_p)/\hbar\omega$ with $\tilde{I}_p = 10.5$ eV.

fixed intensity, $\Delta\tilde{I}_p/\omega$ itself would depend on λ . Therefore, if the modulation period $\delta\lambda$ corresponds to $\delta R = 1$ for the true I_p , any other choice of \tilde{I}_p different from I_p cannot shift all the peaks uniformly to integer values of R .

In a further step, we enumerate all the principal peaks in Fig. 1 (b) from $p = 15$ to 117, and plot the CC number R_p as well as the mismatch to the nearest integer,

$$\Delta R_p \equiv R_p - [R_p], \quad (6)$$

of each peak in Fig. 8. The slope of the line fitted to the data calculated with true I_p (filled circles in Fig. 8(a)) is nearly equal to unity (≈ 1.00), while those with $\tilde{I}_p = 10.5$ eV (diamonds in Fig. 8(a)) have a slope smaller than unity. Moreover, although some fluctuation is seen, the values of ΔR_p are roughly constant, most of them being distributed between 0.3 and 0.6.

As can be seen from Figs. 2–6, the harmonic yields ΔY are not only composed of peaks separated by $\delta R = 1$, but also often contain finer structures with sub-peaks. This is even more so for longer pulses. In order to extract

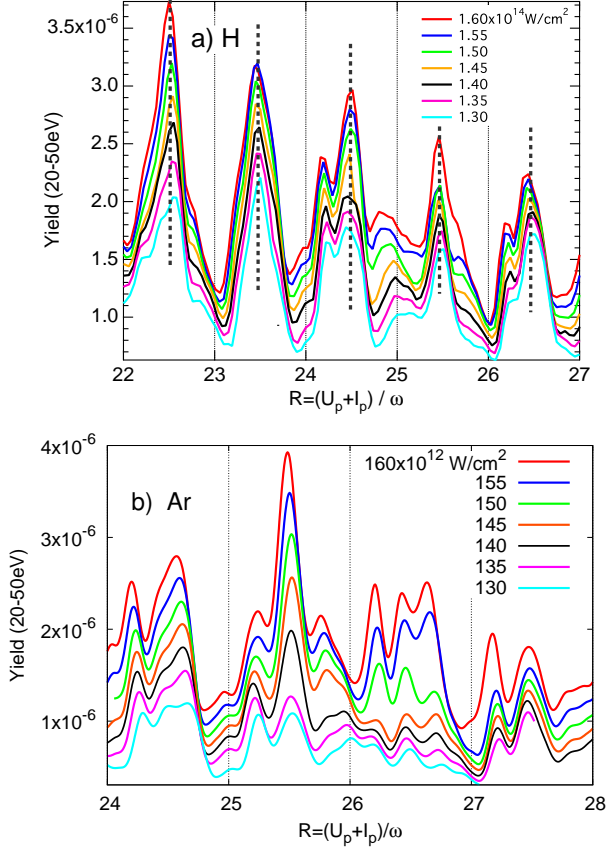


FIG. 6: (Color online) Wavelength dependence of the integrated harmonic yield (20 to 50 eV) in the range of $\lambda \approx 1000 - 1100$ nm, expressed in terms of R , for a) H and b) Ar, for 8-cycle flat-top pulses for different intensities indicated in the figure.

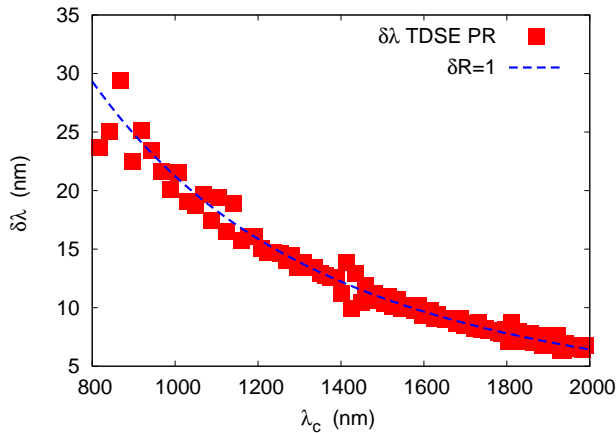


FIG. 7: (Color online) Variation of the modulation period $\delta\lambda$ with the driver central wavelength λ_c for atomic hydrogen. ■: TDSE, dashed line: $\delta R = 1$ (Eq. (7)).

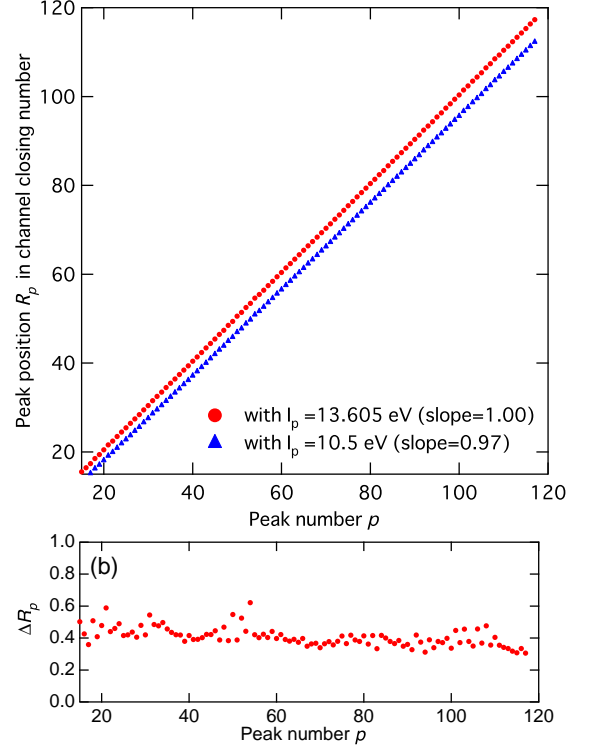


FIG. 8: (Color online) Position R_p of the principal peaks ($p = 15 - 117$) from Fig. 1(b). ■: $(U_p + I_p)/\hbar\omega$ with the true $I_p = 0.5$ a.u. (13.605 eV), ▲: $(U_p + \tilde{I}_p)/\hbar\omega$ with $\tilde{I}_p = 10.5$ eV. The slope obtained by line fitting is also indicated. (b) Corresponding ΔR_p values (Eq. (6)) with the true $I_p = 0.5$ a.u..

the periodicity of these structures quantitatively we calculate the power spectrum of $\Delta Y(R) \times \lambda^{5.3}$ where the multiplication by $\lambda^{5.3}$ removes the smooth global decay (Fig. 1 (b)). We can clearly identify the sharp dominant frequency component precisely at $\Omega = 1$, corresponding to $\delta R = 1$. A beat-like structure of a period of ≈ 20 seen in Fig. 1 (b) gives rise to an additional small side band.

The Fourier spectrum clearly underscores that the peak separation corresponds to $\delta R = 1$ throughout the entire wavelength range between 800 nm and 2 μm . This spacing is closely related to the spacing $\delta\lambda$ in the wavelength dependence of the peak positions. Hence, we can derive the scaling of $\delta\lambda$ with λ to obtain,

$$\begin{aligned} \delta\lambda &= \frac{\text{const.}}{I_p + 3U_p}, \\ &= \frac{1240}{I_p(\text{eV}) + 2.8 \times 10^{-19} I(\text{W/cm}^2) \lambda^2(\text{nm})} \text{nm}. \end{aligned} \quad (7)$$

Equation 7 reproduces the TDSE-calculated λ dependence of $\delta\lambda$ quite well (Fig. 7).

The present results as well as those in Sec. IV strongly indicate that the wavelength and intensity dependence of the HHG yield calls for an explanation in terms of R

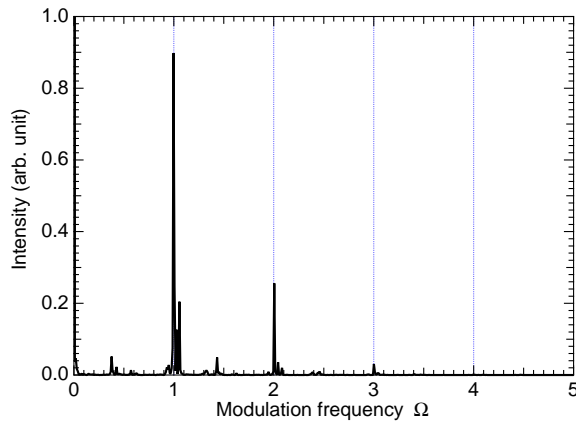


FIG. 9: Power spectrum of $\Delta Y(R) \times \lambda^{5.3}$ (see Fig. 1 (b)).

calculated from the true I_p in spite of the pronounced shift of the peak position from integer R values.

VI. PEAK SHIFT FROM INTEGER R VALUES

While the peak separation is given by $\delta R = 1$, enhancements do not appear at $R = N$, with N being an integer but shifted by an amount ranging from 0.3 to 0.6 (see Fig. 8 (b)). This is in clear contrast to the SFA prediction for the CC peaks in the literature [18] as well as to our present SFA results in Figs. 2 (b)(c) and 3 (b). The fundamental difference between the SFA and the full solution of the TDSE is - apart from numerical or analytical solution strategies - that, in the former one neglects the excited states and the effect of the atomic potential to continuum electrons, which may be a serious deficiency for long-range potentials such as the Coulomb potential. Recent studies on ionization dynamics and doubly-differential photoelectron momentum distributions of hydrogen have shown the significance of the long-ranged Coulomb potential in laser-atom interaction and have illustrated the failure of the SFA near the threshold [35, 36].

A. Truncated Coulomb potential

In order to explore the significance of the long tail of the Coulomb potential for the present case of interferences in the HHG yield, we perform calculations with a truncated Coulomb potential, given by

$$V_{eff}(r, r_c) = \begin{cases} -\frac{1}{r} & (r < r_c) \\ -\frac{e^{-(r-r_c)/r_d}}{r} & (r > r_c) \end{cases}, \quad (8)$$

where the effective range of the truncated Coulomb potential r_c is varied between $r_c = 10$ and $r_c = 70$ a.u.

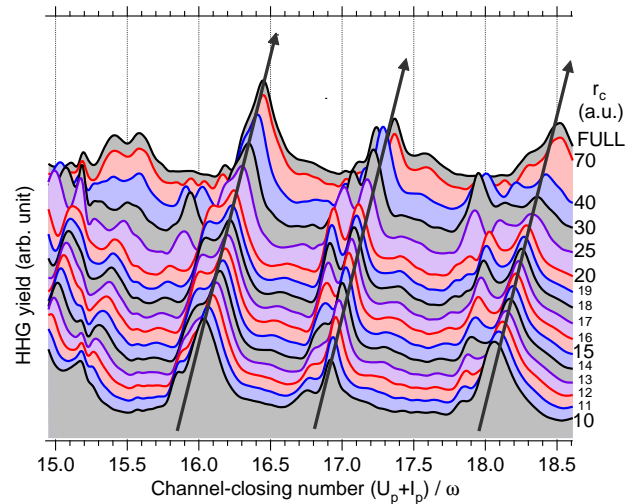


FIG. 10: (Color online) Comparison of the wavelength-dependence $800 \text{ nm} < \lambda_c < 900 \text{ nm}$ of the harmonic yield ΔY for H, expressed in terms of R , calculated with the full Coulomb potential (marked as “FULL”) with the truncated Coulomb potentials for varying values of r_c as indicated. The pulse has a 16-cycle flat-top shape, other pulse parameters are the same as in Fig. 1.

and the width of the cross-over region r_d is chosen to be $r_d = 10$ a.u.. For these parameter values, the ionization potential and the first excitation energy remain unchanged to an accuracy of $\approx 10^{-9}$ and $\approx 10^{-3}$, respectively. It should be noted that the classical electron quiver motion amplitude is $\alpha_q = 26.3$ a.u. for $I = 1.6 \times 10^{14} \text{ W/cm}^2$ and $\lambda_c = 900 \text{ nm}$, and $\alpha_q = 39.3$ a.u. for $\lambda_c = 1100 \text{ nm}$.

We thus explore the entire range from $r_c/\alpha_q \approx 0.3$ to $r_c/\alpha_q \approx 2.3$. Convergence to the solution employing the full Coulomb potential is reached only for r_c as large as 70 a.u. (see Figs. 10 and 11). Most important in the present context is a systematic, almost rigid shift of the peaks as a function of r_c . Only for small r_c (≈ 10 a.u.), the maxima are found near channel closings (near R equal to an integer), in agreement with the SFA results [18]. This observation indicates that the Coulomb potential is indeed responsible for a - to first approximation - monotonic and nearly uniform shift of the peaks. It should be noted that the long-ranged Coulomb potential manifests itself in two seemingly different effects. Firstly, it supports high-lying Rydberg states which converge to the continuum at threshold. Furthermore, Coulomb scattering and deflection influences the motion of the returning electron, even at large distances from the core.

B. Effective ionization potential

The influence of the potential form on the position of the CC was previously identified within the framework of a 1D-TDSE model [33, 34]. It was suggested

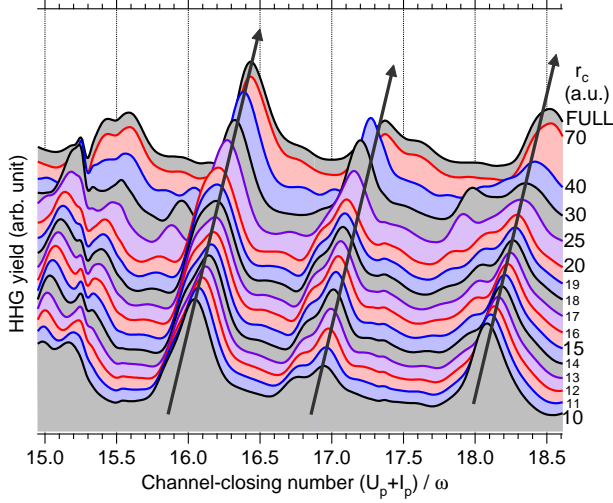


FIG. 11: (Color online) Same as Fig. 10, but for a pulse length of 8 cycles (flat-top).

to use an “effective” ionization potential \tilde{I}_p in Eq. (1) when comparing TDSE calculation with models employing zero-range potentials to account for high-order above-threshold ionization (ATI) spectra at $R \neq N$ [31]. Employing an effective ionization potential \tilde{I}_p in an SFA model roughly leads to a rigid horizontal shift of the interference structure of the HHG yield, in accordance with our observations in Figs. 10 and 11.

Different lines of arguments are invoked for employing \tilde{I}_p rather than I_p . However, they all have in common that the existence of a strongly distorted, continuum-like excited state ε_n is considered responsible for an effectively lower ionization threshold. For convenience, let us therefore define $\Delta\tilde{I}_p \equiv \tilde{I}_p - I_p$, which is expected to be a negative quantity ($\Delta\tilde{I}_p < 0$). Different choices of $\Delta\tilde{I}_p$ are explored. Faria *et al.* [33] argue that ε_n should be given by the condition that its radius $r_n \approx 3n^2/2$ for principal quantum number n should match the quiver amplitude $\alpha_q = F_0/\omega^2$. Together with the Rydberg energy $\varepsilon_n \approx -I_p/n^2$ this would imply

$$\Delta\tilde{I}_p \approx -\frac{3\omega^2}{2F_0} I_p \propto I^{-1/2} \lambda^{-2}. \quad (9)$$

Accordingly, the change of the effective ionization potential, $\Delta\tilde{I}_p$, becomes wavelength dependent. On the other hand, we have found a fairly rigid equidistance $\delta R = 1$ as well as a nearly constant shift ΔR of the latter away from the integers over a wide range of λ_c . Consequently, if we assume that $\Delta\tilde{I}_p$ compensates for ΔR_p , these quantities must satisfy the relation $\Delta\tilde{I}_p = -(\Delta R_p + m)\hbar\omega$, with m being a possible integer offset and ΔR_p defined in Eq. (6). Figures 10 and 11 clearly show that the amount of the peak shift in R is smaller than unity, hence $m = 0$. This leads to

$$\Delta\tilde{I}_p = -\Delta R_p \hbar\omega \propto \lambda^{-1}, \quad (10)$$

Obviously, hypothesis Eq. (9) is not consistent with Eq. (10). In addition, no upper limit for $\Delta\tilde{I}_p$ according to Eq. (9) was discussed in literature. This may lead to the obviously incorrect conclusion that $\Delta\tilde{I}_p \rightarrow 3.4$ eV as soon as in a low intensity and low wavelength limit the $n = 2$ Rydberg state (or even the ground state!) would govern the effective threshold invoked.

An alternative proposal put forward by Frolov *et al.* [7] relates the energy ε_n to the formation of an effective continuum by broadening of the level with principal quantum number n . Accordingly, ε_n is determined by the condition $\Gamma_n = \Delta\varepsilon_n$, where the width Γ_n (related to ionization rate) approaches the level spacing $\Delta\varepsilon_n$. While in the limit of quasi-static tunneling, the tunneling rate $\Gamma_n \propto \exp[-2(2|\varepsilon_n|)^{3/2}/(3F_0)]$ strongly depends on the field strength F_0 , but only very weakly on λ . The resulting value of $\Delta\tilde{I}_p$ is estimated to be -3.1 eV for atomic hydrogen and $I = 1.6 \times 10^{14}$ W/cm² in Ref. [7]. This does not meet the condition Eq. (10), according to which $|\Delta\tilde{I}_p|$ should be smaller than the photon energy $\hbar\omega$ (1.5 eV in the present parameter range) of the driving laser pulse.

Moreover, with the help of Eq. (10) we can determine the effective parameter dependence of $\Delta\tilde{I}_p$ employing the numerical values for ΔR over a wide range of λ_c and F_0 (Fig. 12). Our results suggest a weak dependence of \tilde{I}_p on both the wavelength and the intensity, the latter being roughly proportional to $\lambda^{-0.3}$. This supports neither the explanations of Frolov *et al.* nor of Faria *et al.*

C. Coulomb-corrected classical trajectory model

In addition to the ability to support (an infinite number) excited bound states, the Coulomb potential affects the propagation of the rescattering electron which is neglected in the SFA as well. As the quantum interference of electron trajectories is responsible for the oscillation in the harmonic yield, their distortion by the potential may be crucial.

In SFA, the time-dependent dipole moment $d(t)$ can be expressed as [29]

$$d(t_f) = \sum_{P(t_i)} b_{\text{ion}}(t_i) \cdot e^{-iS_P(t_i, t_f, I_p)} \cdot c_{\text{rec}}(t_f) + \text{c.c.}, \quad (11)$$

i.e., a sum over paths P that start at the moment of tunnel ionization t_i with amplitude $b_{\text{ion}}(t_i)$, evolve in the laser field - acquire the phase $e^{-iS_P(t_i, t_f)}$ - and recombine upon rescattering at the core at time t_f with the amplitude $c_{\text{rec}}(t_f)$. The interference oscillations in the HHG yield are controlled by the semiclassical action S_P of the path P , which reads:

$$S_P(t_i, t_f, I_p) = \int_{t_i}^{t_f} \frac{(p + A(t'))^2}{2} dt' + I_p(t_f - t_i), \quad (12)$$

where $A(t)$ is the laser vector potential, and p is the classical momentum of the returning trajectory. The effect of

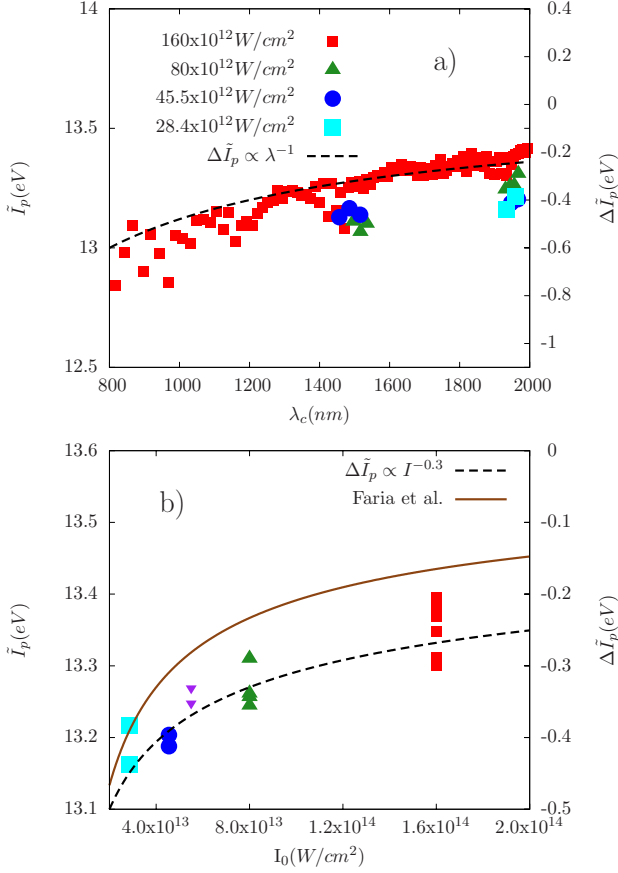


FIG. 12: (Color online) \tilde{I}_p (left axis) and $\Delta\tilde{I}_p$ (right axis) as obtained from Eq. (10) for a broad range of driver wavelength and various intensities. **a)** as function of λ_c , **b)** as function of intensity near $\lambda_c = 1950$ nm. The solid line compares to the prediction of Faria *et al.* [33], while the dashed line shows a power law fit to our data ($\Delta\tilde{I}_p \propto I^{-0.3}$).

the Coulomb potential can be incorporated into Eq. (12) with help of an eikonal approximation as a correction to the (action) phase with [29],

$$\Delta S_P(t_i, t_f) = \int_{t_i}^{t_f} V_{EI}(r(t')) dt'. \quad (13)$$

Clearly, the eikonal approximation would fail at small distances from the nucleus. This difficulty can be bypassed using the observation (Sec. VI A) that at a cut-off $r_c = 10$ a.u. the SFA limit of channel closings at integer values of R is reached. Consequently, we set

$$V_{EI}(r) = V_{eff}(r, r_c = \infty) - V_{eff}(r, r_c = 10) \quad (14)$$

when calculating the long-range phase correction.

We evaluate Eq. (13) along classical trajectories in the laser electric field $F(t)$, confined in the xy -plane, starting and ending at the “tunnel exit” $z_0 = I_p/F_0$. Trajectory modifications due to the Coulomb potential are small and can be neglected to first approximation [29], i.e., we use the same sets of (t_i, t_f) as in Eq. (12).

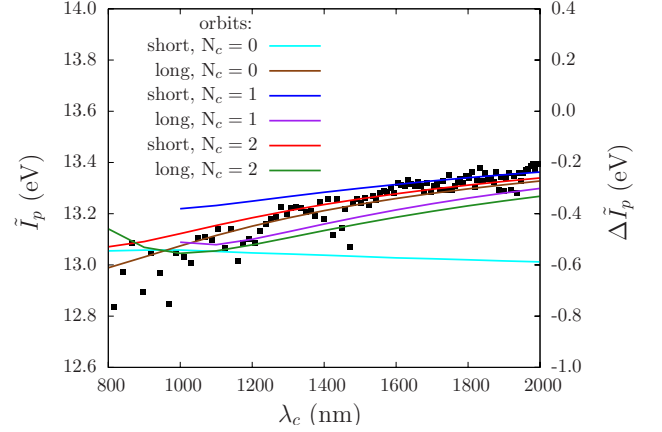


FIG. 13: (Color online) \tilde{I}_p (left axis) and $\Delta\tilde{I}_p$ (right axis) as a function of driver wavelength, employing Eq. 15 and the potential of Eq. 14. Intensity is $I = 1.6 \times 10^{14}$ W/cm². Lines stem from the six shortest orbits recolliding with 20eV, revisiting the core N_c (here: zero, one, or two) times before recombining (as indicated). For each energy and each N_c , a short and a long orbit exist. ■: TDSE data (see also Fig. 12).

It is now suggestive to express this additional phase in terms of a change in the “effective ionization potential”, \tilde{I}_p . Accordingly,

$$\Delta\tilde{I}_p = \Delta S_P(t_i, t_f)/(t_f - t_i). \quad (15)$$

Figure 13 shows \tilde{I}_p obtained by Eq. 15 for several (the shortest) classical trajectories which contribute to the harmonics near 33.6 eV (hence near the center of the HHG yield range considered in this work).

Remarkably, most trajectories (save the shortest one) behave qualitatively very similarly. In spite of its oversimplification, this Coulomb-corrected model explains the behavior of \tilde{I}_p even quantitatively well, which is a strong indication that the effect of the Coulomb potential on the rescattering electronic motion is key to the understanding of the apparent peak shift in the wavelength-dependence of the HHG yield.

VII. CONCLUSIONS

Using full numerical solutions of the time-dependent Schrödinger equation, we have found that the fundamental wavelength dependence of HHG with few-cycle pulses in the single-atom response features surprisingly strong oscillations on fine wavelength scales with modulation periods as small as 6 nm in the mid-infrared regime near $\lambda = 2\mu\text{m}$. Thus, even a slight change in fundamental wavelength leads to strong variations in the HHG yield. This fine-scale rapid variation is the consequence of the interference of several rescattering trajectories with long excursion times, confirming the significance of multiple returns of the electron wavepacket [14].

The present oscillations are closely related to similar regular peak-like enhancements of harmonic yield as a function of intensity I_0 [15, 16, 17, 18], previously discussed in connection with channel closings. Our analysis of the simultaneous wavelength-intensity-dependence has revealed that the spacing between adjacent peaks (expressed in terms of the channel closing number R) is very accurately given by $\delta R = 1$ over a wide range of λ and I_0 . This corresponds to the spacing of adjacent channel closings as predicted by the strong-field approximation (e.g. [18]). The condition $\delta R = 1$ holds only if R is defined with the true ionization potential. However, the peak positions are significantly shifted relative to integer values. The parametric dependence of the peak shift on the wavelength λ and the intensity I_0 has been investigated. Our analysis shows that this peak shift can be accounted for by the effects of the Coulomb tail on the motion of the returning electron.

Acknowledgments

The work was supported by the Austrian “Fonds zur Förderung der wissenschaftlichen Forschung”, under grant no. FWF-SFB016 “ADLIS”. K.S. also acknowledges support by the IMPRS-APS program of the MPQ (Germany). K.L.I. gratefully acknowledges financial support by the Precursory Research for Embryonic Science and Technology (PRESTO) program of the Japan Science and Technology Agency (JST) and by the Ministry of Education, Culture, Sports, Science, and Technology of Japan, Grant No. 19686006. K.L.I. would like to thank P. Salières, T. Augustine, and H. Suzuki for illuminating discussions.

-
- [1] J. Seres, E. Seres, A.J. Verhoef, G. Tempea, Ch. Streli, P. Wobrauschek, V. Yakovlev, A. Scrinzi, Ch. Spielmann, and F. Krausz, *Nature (London)* **433**, 596 (2005).
 - [2] M. Hentschel, R. Kienberger, Ch. Spielmann, G. Reider, N. Milosevic, T. Brabec, P. Corkum, U. Heinzmann, M. Drescher, and F. Krausz, *Nature (London)* **414**, 509 (2001).
 - [3] G. Tsakiris, P. Tzallas, D. Charalambidis, N. Papadogiannis, and K. Witte, *Nature (London)* **426**, 267 (2003).
 - [4] T. Sekikawa, A. Kosuge, T. Kanai, and S. Watanabe, *Nature (London)* **432**, 605 (2004).
 - [5] Y. Nabekawa, H. Hasegawa, E.J. Takahashi, and K. Midorikawa, *Phys. Rev. Lett.* **94**, 043001 (2005).
 - [6] K. Schiessl, K.L. Ishikawa, E. Persson, and J. Burgdörfer, *Phys. Rev. Lett.* **99**, 253903 (2007).
 - [7] M.V. Frolov, N.L. Manakov, and A.F. Starace, *Phys. Rev. Lett.* **100**, 173001 (2008).
 - [8] K. Schiessl, K.L. Ishikawa, E. Persson, and J. Burgdörfer, *J. Mod. Opt.* **55**, 2617 (2008).
 - [9] E.J. Takahashi, T. Kanai, K.L. Ishikawa, Y. Nabekawa, and K. Midorikawa, *Phys. Rev. Lett.* **101**, 253901 (2008).
 - [10] P. Colosimo, G. Doumy, C. I. Blaga, J. Wheeler, C. Hauri, F. Catoire, J. Tate, R. Chirila, A.M. March, G.G. Paulus, H.G. Muller, P. Agostini, and L.F. DiMauro, *Nature Phys.* **4**, 386 (2008).
 - [11] M. Lewenstein, Ph. Balcou, M.Yu. Ivanov, A. L’Huillier, and P.B. Corkum, *Phys. Rev. A* **49**, 2117 (1994).
 - [12] A. Gordon and F. Kärtner, *Opt. Express* **13**, 2941 (2005).
 - [13] B. Shan and Z. Chang, *Phys. Rev. A* **65**, 011804(R) (2001).
 - [14] J. Tate, T. Augustine, H.G. Muller, P. Salières, P. Agostini, and L.F. DiMauro, *Phys. Rev. Lett.* **98**, 013901 (2007).
 - [15] E.S. Toma, Ph. Antoine, A. de Bohan, and H.G. Muller, *J. Phys. B* **32**, 5843 (1999).
 - [16] A. Zair, M. Holler, A. Guandalini, F. Schapper, J. Biegert, L. Gallmann, U. Keller, A. S. Wyatt, A. Monmayrant, I. A. Walmsley, E. Cormier, T. Augustine, J. P. Caumes, and P. Salières, *Phys. Rev. Lett.* **100**, 143902 (2008).
 - [17] B. Borca, A.F. Starace, A.V. Flegel, M.V. Frolov, and N.L. Manakov, *Phys. Rev. A* **65**, 051402(R) (2002).
 - [18] D.B. Milošević, and W. Becker, *Phys. Rev. A* **66**, 063417 (2002).
 - [19] H.G. Muller and F.C. Kooiman, *Phys. Rev. Lett.* **81**, 1207 (1998).
 - [20] K.C. Kulander, K.J. Schafer, and J.L. Krause, in *Atoms in intense laser fields*, M. Gavrila, ed. (Academic, New York, 1992) pp. 247–300.
 - [21] J.L. Krause, K.J. Schafer, and K.C. Kulander, *Phys. Rev. A* **45**, 4998 (1992).
 - [22] X.-M. Tong and S. Chu, *Chem. Phys.* **217**, 119 (1997).
 - [23] K. Schiessl, E. Persson, A. Scrinzi, and J. Burgdörfer, *Phys. Rev. A* **74**, 053412 (2006).
 - [24] W.H. Press, S.A. Teukolsky, W.T. Vetterling, and B.P. Flannery, *Numerical Recipes* (Cambridge University Press, Cambridge, 1992).
 - [25] J.D. Jackson, *Classical Electrodynamics* (John Wiley & Sons, New York, 1998).
 - [26] M.L. Du and J.B. Delos, *Phys. Rev. Lett.* **58**, 1731 (1987).
 - [27] P. Salières, B. Carré, L. Le Déroff, F. Grasbon, G.G. Paulus, H. Walther, R. Kopold, W. Becker, D.B. Milošević, A. Sanpera, and M. Lewenstein, *Science* **292**, 902 (2001).
 - [28] P.B. Corkum, *Phys. Rev. Lett.* **71**, 1994 (1993).
 - [29] M.Yu. Ivanov, T. Brabec and N. Burnett, *Phys. Rev. A* **54**, 742 (1996).
 - [30] V.S. Yakovlev and A. Scrinzi, *Phys. Rev. Lett.* **91**, 153901 (2003).
 - [31] R. Kopold, W. Becker, M. Kleber, and G. G. Paulus, *J. Phys. B* **35**, 217 (2002).
 - [32] H. G. Muller, *Phys. Rev. A* **60**, 1341 (1999).
 - [33] C. Figueira de Morisson Faria, R. Kopold, W. Becker, and J.M. Rost, *Phys. Rev. A* **65**, 023404 (2002).
 - [34] R. Taïeb, V. Vénier, J. Wassaf, and A. Maquet, *Phys. Rev. A* **68**, 033403 (2003).
 - [35] D.G. Arbó, S. Yoshida, E. Persson, K.I. Dimitriou, and J. Burgdörfer, *Phys. Rev. Lett.* **96**, 143003 (2006).
 - [36] D.G. Arbó, J.E. Miraglia, M.S. Gravielle, K. Schiessl, E. Persson, and J. Burgdörfer, *Phys. Rev. A* **77**, 013401 (2008).

(2008).